International Journal of Heat and Mass Transfer 54 (2011) 5139–5148

Contents lists available at SciVerse ScienceDirect

International Journal of Heat and Mass Transfer

journal homepage: www.elsevier.com/locate/ijhmt

Bubble nucleation in microchannel flow boiling using single artificial cavity

Jae Yong Lee [a], Moo-Hwan Kim [b], Massoud Kaviany [c], Sang Young Son [a,*]

[a] Department of Mechanical Engineering, University of Cincinnati, OH 45221, USA
[b] Department of Mechanical Engineering, POSTECH, Kyungbuk 790-874, Republic of Korea
[c] Department of Mechanical Engineering, University of Michigan, Ann Arbor, MI 48109, USA

ARTICLE INFO

Article history:
Received 27 December 2010
Received in revised form 29 April 2011
Accepted 29 April 2011

Keywords:
Visualization
Flow boiling
Bubble incipience
Bubble detachment
Bubble growth rate
Microchannel

ABSTRACT

Microchannel ($D_h \leqslant 100$ μm) water flow boiling under low mass flux ($G \leqslant 138.9$ kg/(m^2 s)) is presented to investigate the local phenomena of flow regime development and nucleating bubble growth rate. During horizontal flow, onset of nucleation, flow regime, and isolated single bubble growth and detachment from a single artificial cavity were observed and analyzed by microscopic high-speed visualization under various flow rates and wall superheat conditions. Results showed that while the predictions pertaining to inception by bubble nucleation theory match well, bubble growth rate, detachment and expansion in a microchannel differs dramatically from a macrochannel.

1. Introduction

There are many applications of nucleate flow boiling due to its large heat removal capability. The efficiency to remove heat can be increased by employing smaller hydraulic diameter channels which use smaller amount of fluid flow. Applications include point-wise cooling for high speed integrated processor and small-size, high power LEDs with 'hot spot junctions' which generate a greater amount of heat than surrounding areas. This may result in malfunction if enough heat is not dissipated through the package to their heat sink [1,2]. Another example can be a cooling plate for fuel cell stack using boiling refrigerant [3,4]. Large area of reaction induces significant temperature differences between center and edge area. If bubble nucleation can be controlled specifically at the hottest location inside the stack layer, it can help maintain a more uniform temperature profile.

In recent years, minichannel and microchannel flow boiling has been studied to understand bubble nucleation conditions and behavior, due to the advantages of large surface-to-volume ratios coupled with phase change have large heat removal capabilities. Several researchers have conducted flow boiling in minichannel and microchannel visualization under various heat and mass flux conditions despite difficulties in control and flow instabilities. Since the early studies on constituting a classification of flow patterns at macroscale [5–7], flow boiling visualization methods have helped the understanding of bubble incipience, growth and detachment behavior inside channels.

Cornwell and Kew conducted detailed experiments in minichannels for classifying the flow regime and obtaining correlations [8]. Kasza and Wambsganss used high-speed visualization to show that confinement effects, flow regimes and heat transfer characteristics are changed in rectangular minichannels at macroscale flow boiling [9,10]. Kandlikar et al. carried out various nucleating bubble visualization experiments in flow boiling using conventional channel [11–13], minichannel [14] and microchannel [15] ($D_h = 207$, 333, $G = 112$–1782). Their results showed how bubbles move and the important parameters which need to be considered. Jiang et al. used triangular and diamond microchannels with visualization window, a partially installed heater and temperature sensors ($D_h = 40$, 80, $G = 22$–129) [16,17]. They presented visual images of single bubble nucleation following heat flux variations and found different boiling characteristics, such as the non-existence of a plateau in the boiling curve and different behavior at the local stage of the bubble. Zhang et al. studied boiling flow in a microchannel, using a single rectangular microchannel with doped-type heater and temperature sensors at the bottom of the channel ($D_h = 45$–113, $G = 123$–160) [18]. They observed flow boiling convection in various ways, such as visualization of single nucleating bubbles and transition to the slug pattern in microchannel. Hetsroni et al. carried out experiments with triangular microchannels ($D_h = 130$, $G = 95$–340) [19], and showed explosive boiling, wetting and re-wetting according to the flow and heat

* Corresponding author. Tel.: +1 513 556 2830; fax: +1 513 556 3390.
E-mail address: sangyoung.son@uc.edu (S.Y. Son).

0017-9310/$ - see front matter © 2011 Elsevier Ltd. All rights reserved.
doi:10.1016/j.ijheatmasstransfer.2011.08.042

Nomenclature

D_h	hydraulic diameter [μm]	ρ	density [kg/m^3]
G	mass flux [kg/(m^2 sec)]	σ	surface tension [N/m]
i	enthalpy [J/kg]		
$\dot{m}$	mass flow rate [kg/sec]	*Subscript*	
R	radius [μm]	b	bubble
T	temperature [°C]	c	cavity
t	time [s]	f	liquid
W	microchannel width [μm]	g	vapor
H	microchannel height [μm]	fg	latent
		min	minimum
Greek symbols		max	maximum
δ	thermal boundary layer thickness [μm]	sat	saturation
θ	contact angle [°]	sub	subcooled

transfer conditions. Liu et al. conducted experiments with microchannels and developed analytical modeling to match the onset of boiling temperature (D_h = 384, G = 498–899) [20]. They showed single bubble growth, detachment behavior and growth rate, however no explosive boiling was reported due to the relatively large channel size and mass flux. Lee et al. used trapezoidal (D_h = 41.3, G = 170–477) and rectangular microchannels (D_h = 33.7, G = 417–625) to investigate bubble nucleation. They conducted measurements on bubble growth rate and departure radius at various heat and mass flux [21], and tried to investigate eruptive boiling with high-speed visualization [22]. Liu et al. used a seed bubble generator instead of a cavity in order to make boiling incipience in the triangular microchannels (D_h = 100, G = 378–898). Their results showed that a relationship exists between flow patterns and heat transfer enhancement depending upon the bubble generation frequency [23].

Most of aforementioned research mainly studied using multiple microchannels and high mass flux conditions. A multiple microchannel structure is useful for flow boiling applications, but makes it difficult to have uniform flow rate in each channel. Once vapor blocks the channel, flow maldistribution becomes more severe. Although high mass flux can help to maintain the uniform flow, it requires high inlet pressure and thick fixture housing. Consequently acquiring clear, high magnification images becomes limited and local boiling nucleation phenomena becomes difficult to be investigated in detail. In addition, most of flow boiling research faced similar problems in terms of uncontrollable boiling behavior because the incipience location is randomly present. Generally bubble nucleating point is decided by the combined effects of inlet fluid temperature, wall superheat temperature, flow rate, and size of natural defects in the channel. There has been limited number of studies where authors have tried to use internal structures, such as multiple notches and cavities in order to enhance nucleation flow boiling [18,24–26]. Although these internal structures helped to initiate bubbles, isolation of sources that affect bubble growth behavior has been found to be difficult.

The objective of this study is investigating the local phenomena of flow regime development and nucleating bubble growth rate. This effort is conducted by associating local thermodynamic conditions and high speed visualization images to see the transient event in detail. Using a single microchannel under the conditions of $G \leqslant 138.9$ kg/(m^2 s), onset of nucleating boiling, subsequent bubble growth behavior and flow boiling pattern were observed by high-speed visualization. The present work can be used to obtain a more extensive understanding of microchannel flow boiling than is available from previous results [27]. To this end, we developed a thermofluidic microelectromechanical systems (MEMS) device which integrates a single microchannel, a heater, temperature sensors, and a visualization window. For establishing controllability and repeatability, a single artificial cavity was fabricated at the bottom of the microchannel. High-speed, high resolution visualization coupled with local temperature measurements helped to classify bubble incipience and growth behavior according to the conditions.

2. Description of the experiment

2.1. Integrated micro thermofluidic MEMS device setup

An integrated micro thermofluidic MEMS device comprising of a single microchannel, a heater, temperature sensors and a visualization window was designed and fabricated. The schematic of the device is illustrated in Fig. 1. The silicon-based, dry-etched single microchannel had either a square or rectangular cross-section, with dimensions varying from 50 to 100 μm. A micro line heater, located at the bottom and covering most of the channel was used to apply constant heat fluxes corresponding to various boiling conditions associated with flow rates, cavity diameter, and channel

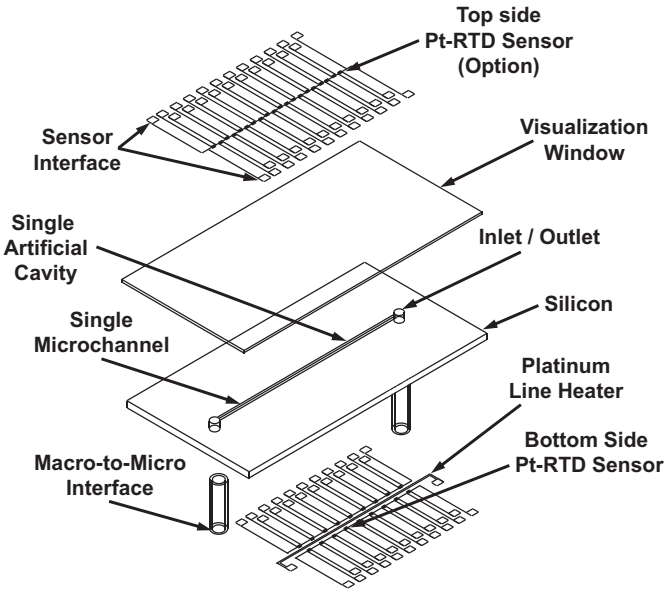

Fig. 1. Schematic of micro thermofluidic MEMS device integrating a microchannel, visualization window, Pt-RTD sensor and platinum heater.

Table 1
Detailed specification of micro thermofluidic MEMS device.

Parts		Dimension	Description
Microchannel	# of channel	1	Silicon
	Width	50, 100 μm	(Square or Rectangular)
	Height	46, 48, 100 μm	
	Length	64 mm	
Visualization window	Thickness	170 μm	Pyrex, top side
Artificial cavity	Radius	12.5 – 16.4 μm	Bottom of the microchannel
	Location	24 mm from inlet	
Line heater	Width	102 μm	Platinum line
	Length	35 mm	
Top side temp. sensor	Size	100 × 115 μm (W 100 μm)	
	Quantity 41 (Single line)		100 Ω Pt-RTD
Lower side temp. sensor	Size	100 × 115 μm (W 100 μm)	100 Ω Pt-RTD
	Quantity	39 (Double lines)	

geometry. To measure the wall/fluid temperature, a 100 Ω serpentine Platinum Resistance Temperature Detector (Pt-RTD) was designed and optimized for linearity, stability and sensitivity. The lower side of the Pt-RTD sensors was located on both sides of the heater, allowing for recording of local temperature profiles along the microchannel. On the top, a 170 μm thick Pyrex™ transparent window was used to investigate the bubble behavior, and the top side of the Pt-RTD sensors was fabricated along the channel. Even though these sensors covered the microchannel window, thin serpentine shape of sensors and window coupled with high magnification and a high numerical aperture lens allowed for distinguishing the edge line of growing bubble. In the case of measuring bubble growth rate, microchannel with a single artificial cavity was custom fabricated to create a nucleation control spot at the bottom of the microchannel. It was located at one-third of the channel inlet, and had a conical inlet and cylindrical body shape because of isotropic etching characteristics. The aforementioned design parameters are listed in Table 1. For manufacturing the device, fabrication processes including artificial cavity fabrication were largely divided into three parts: deep reactive ion etching (RIE) of the artificial cavity and microchannel into a silicon substrate, glass fabrication for the visualization window, and sputtering for integrating the heater and sensors on both sides. Fig. 2 presents the abbreviated fabrication process diagram including fabrication of single artificial cavity.

2.2. Experimental test setup

The experimental test setup was designed to acquire consecutive visual images and thermodynamic properties simultaneously. As shown in Fig. 3, the integrated device is located at top of the optical microscope stage (Axioskope II, Carl Zeiss Inc.). Depending on the bubble growth speed, visual images were acquired by the combination of two different types of CCD cameras and two different light sources. Among the camera setups, the first visualization setup was comprised of a high-speed CCD camera capable of recording sequential high-speed images up to 1825 frames per second (HCC1000, Vosskühler GmbH), using a continuous mercury lamp for a 500 μs minimum exposure time. The second visualization setup involved a high-speed camera, which could record two images with a 200 ns minimum time interval (FM3S, LaVision GmbH) and two resonance Nd:YAG laser with a 4 ns illumination time (MiniLase III, New Wave Research Inc.). The illumination and time interval between images could be adjusted by tuning the laser using frame straddling technique. Pair of clear images could be acquired at 4 ns laser illumination time with various time

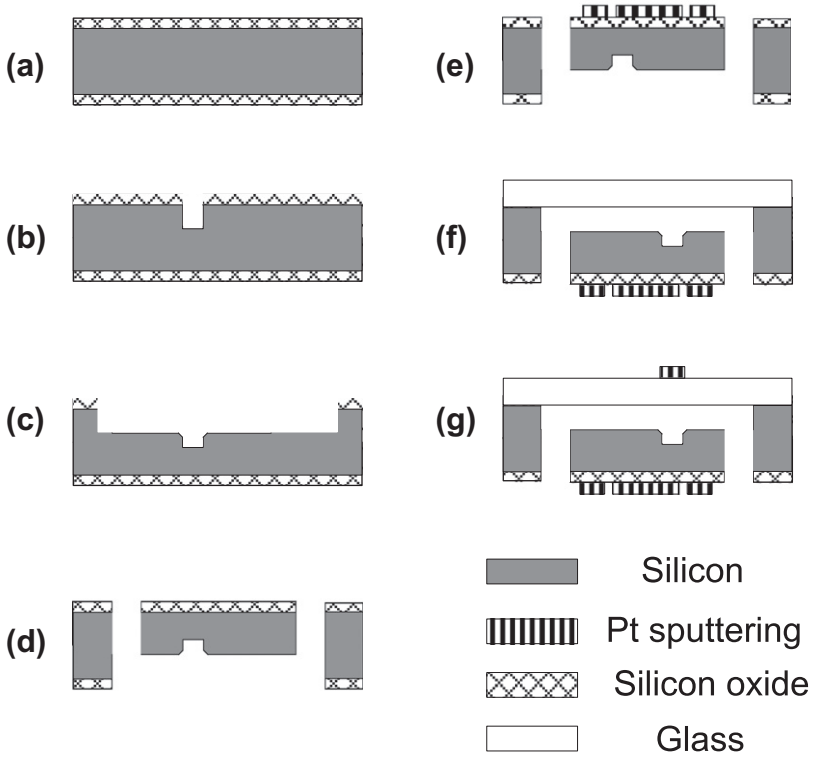

Fig. 2. Microfabrication process: (a) Thermal oxidation of double-side polished silicon, (b) dry etching of single cavity, (c) dry etching of microchannel, (d) dry etching of fluidic interface on back side, (e) Pt sputtering for heater and bottom side RTD sensor, (f) Glass-silicon anodic bonding and (g) Pt sputtering for top side RTD sensor.

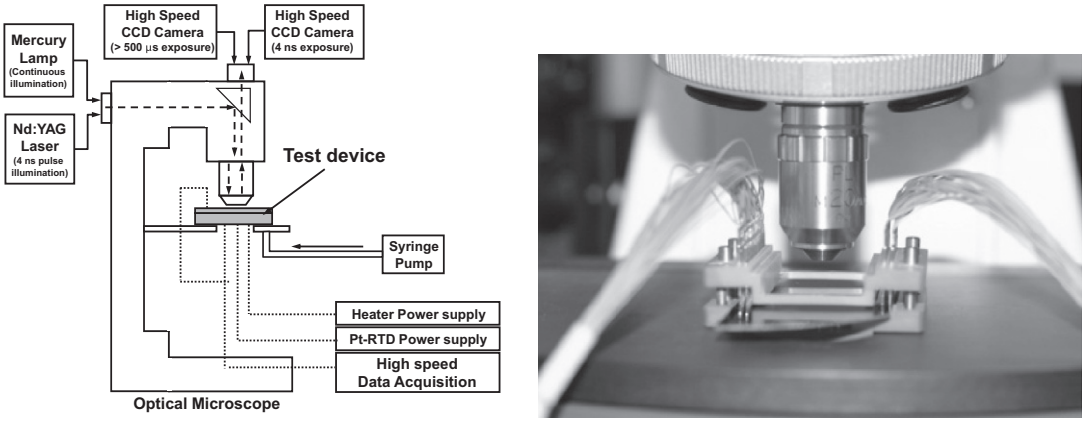

Fig. 3. Schematic diagram of the experimental test setup.

intervals. Data acquisition main frames (34970A, Agilent Co.) with high-speed multiplexer submodules (34902A, Agilent Co.) were used to gather local temperatures. Two DC power supplies were used for the micro line heater (3620A, Agilent Co.), and another sets of programmable DC power supplies (7651, YOKOGAWA Instrument) for the RTD sensors. A high precision syringe pump (PHD2000, Harvard Instrument Co.) and glass syringe (GASTIGHT, Hamilton Co.) maintained the programmed flow rates. The working fluid was degassed, and deionized water, and the inlet subcooled temperature was maintained at 24 ± 1 °C. Operating pressure was measured using an absolute pressure transducer (280E, Setra Co.) at the inlet of the device (Fig. 1) while the outlet is open to atmosphere. The measured absolute pressure is in the range from 100.8 to 101.5 kPa during experiments. The corresponding saturated temperature was ranging from 99.83 °C to 100.02 °C.

2.3. Experimental uncertainty

The measurement uncertainty of voltage and current were ±0.005% and ±0.53% respectively and the accuracy of the flow rate was ±1% in terms of set value. The accuracy of the Pt-RTD sensor at the bottom side of the microchannel was measured as ±0.3 °C. Temperatures were measured along the channel and then averaged every one second. At the nearest nucleating point, acquired temperature was adopted as wall superheat temperature Regarding the boiling cases, previous research reported that the surface temperature at the point of nucleation occasionally varied by 11–17 °C in 2 ms [28]. Due to the differences in data processing, rapid fluctuation above mentioned was not described in this experiment. Temperature fluctuation in a single phase stayed within ±0.3 °C, but it rose to ±0.5 °C during boiling. For investigating the boiling phenomena through visualization, device with fluidic and electrical connections were installed on top of the microscope stage as shown in Fig. 3. Objective lenses were closely located to the device for high magnification and a large number of contact probes were placed for RTD sensors. Since the both side of the device was exposed, applied heat was transferred to wires through conduction and natural convention on surfaces. This made the effective heat flux difficult to be defined. Instead of effective heat flux, the nearest of boiling point, time-averaged wall superheat temperature was defined as experimental conditions.

In order to evaluate the radius of bubble in the microchannel, bubble shape and size were measured from recorded images. The reflected rays could affect radius because the volume of gas in the water might be underestimated at large angles of incident light. When estimating the size of a bubble from a recorded image, the volume measurement error exceeds 5% when the angle of incident light is over Π/10 rad [29]. In our high magnification experiment, the angle of light was about Π/6.36 rad, so the bubble volume difference between the actual and measured value there is over 5%.

3. Results and discussion

Understanding the phenomena of nucleating bubble dynamics is important to explain the two-phase behavior in flow boiling. It is well-known that macroscale horizontal flow boiling behavior is consequence of multiple events involving bubble nucleation and agglomeration resulting in development of slug and annular flow [30]. Generally, bubble incipience requires a higher degree of superheat temperature to initiate the bubble from the cavity and strongly depends on cavity size, mass flux and wall superheat condition. When bubble grows, bubble growth period is divided into two regions; Inertial controlled growth in the early stage and heat transfer controlled growth in the later stage. Inertial controlled growth is limited by momentum interaction between bubble and surrounding liquid, heat transfer controlled growth is governed by conduction heat transfer from the surrounding liquid to the interface [30,31].

In this study, we mainly focused on investigating the local phenomena of flow regime development and nucleating bubble growth rate. Most of the experiments were conducted with less than 33.3 kg/(m^2 s), thermodynamic conditions and high speed images were matched at the moment of onset of nucleating and subsequent behavior. For observing the flow regime development, we observed behavior of bubble nucleation in natural cavities which are formed at the corner of microchannel. For analyzing nucleating behaviors such as bubble incipient conditions and bubble growth rate, single artificial cavity was used to initiate nucleate flow boiling.

3.1. Bubble nucleation and flow regime development for varying wall superheat temperature

Fig. 4 compares bubble nucleation and local flow regime development under low mass flux depending on wall superheat temperature. From the square microchannel (W = 100 μm, H = 100 μm) with low mass flux (G = 33.3 kg/(m^2 s)), Fig. 4(a) shows formations and interactions of microscale sized bubbles generated from the natural cavities along the channel. In this condition, wall superheat temperature was ΔT_w = 4 °C at the nearest Pt-RTD sensor. A bubble growing from a cavity reached the size of microchannel in a time period of 70 ms. The earliest nucleating bubble, which achieved

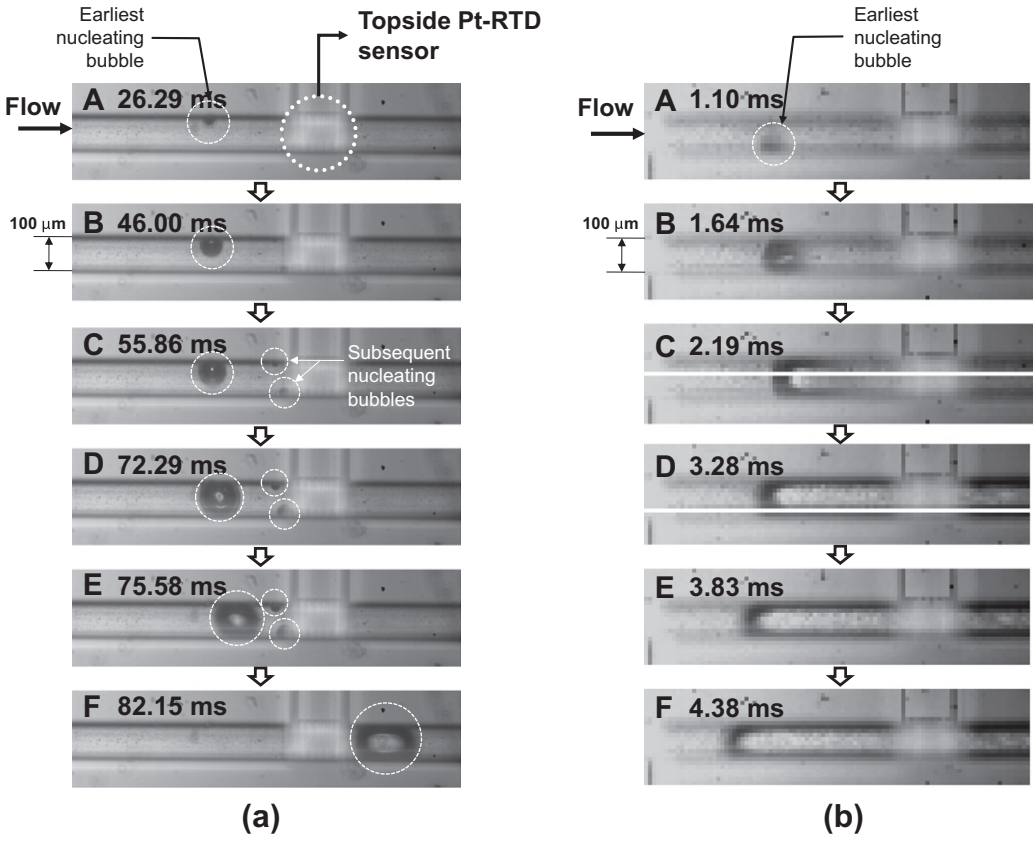

Fig. 4. Flow regime development comparison depending on wall superheat temperature (W = 100 μm, H = 100 μm, G = 33.3 kg/(m^2 s)): (a) bubble nucleation during hundred millisecond (ΔT_w = 4 °C) and (b) explosive bubble nucleation (ΔT_w = 6 °C).

the critical size of detachment, dissociated from the wall and swept along the microchannel interacting with other subsequent growing bubbles (Frame 'D' of Fig. 4(a)). The interaction led to agglomeration of bubbles and merger with multiple other growing bubbles downstream. From the investigation, it is clear that the procedure of flow regime development was similar to the behavior of the minichannel, though some notable differences could be observed during the flow development. In the case of minichannel, it has been reported that channel dimension (1.3–1.5 mm inner diameter) has no confinement effect on bubble growth and departure behavior [33]. However, in our observation the earliest nucleating bubble grew up to the size of hydraulic diameter before detachment. The detached bubble then grows and sweeps along the channel, coalescing with other growing bubbles and impending their growth. Thus the recurring sweep and coalescence play a very important role in governing the entire flow regime.

On the other hand, sequential images in Fig. 4(b) show totally different behavior under the same mass flux with wall superheat temperature ΔT_w = 6 °C. Although the wall temperature was altered only by two degrees, the nucleating behavior changed drastically from Fig. 4(a). A single bubble grew in an explosive manner at the nucleating spot (Frame 'A' of Fig. 4(b)), and it took less than 2 ms to grow up to the size of hydraulic diameter. The growing bubble then expanded upstream to cover the entire channel with thin film. Bubble growth pattern could not be resolved accurately even with 0.55 ms resolution for the visualization method used in the setup. It was evident that bubble growth and detachment pattern showed distinctive features in spite of small differences in wall superheat conditions.

The other noticeable difference was subsequent bubble growth from other cavities, which is located at downstream. From the case of Fig. 4(a), bubbles keep on nucleating from other cavities so that flow regime development was similar to the macroscale flow boiling. On the other hand, Fig. 4(b) showed that the first explosive bubble filled the entire channel resulting in formation of thin film at the channel wall. Since the inception of nucleation requires a larger degree of superheat at liquid thin films, the other cavities became inactive [32]. As a result, the film evaporation governs the thermal transport at the downstream before rewetting occurs, which partly supports the assumptions of microchannel boiling model [34].

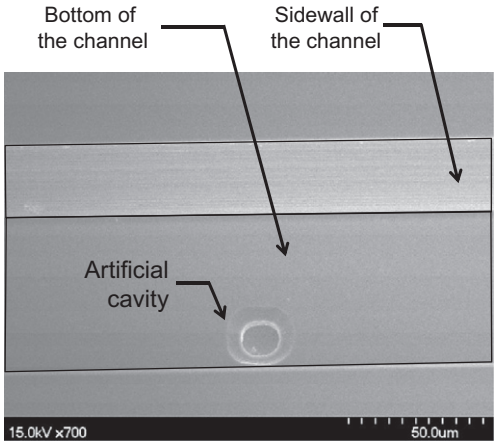

Fig. 5. 700x SEM image of single artificial cavity at the bottom of microchannel.

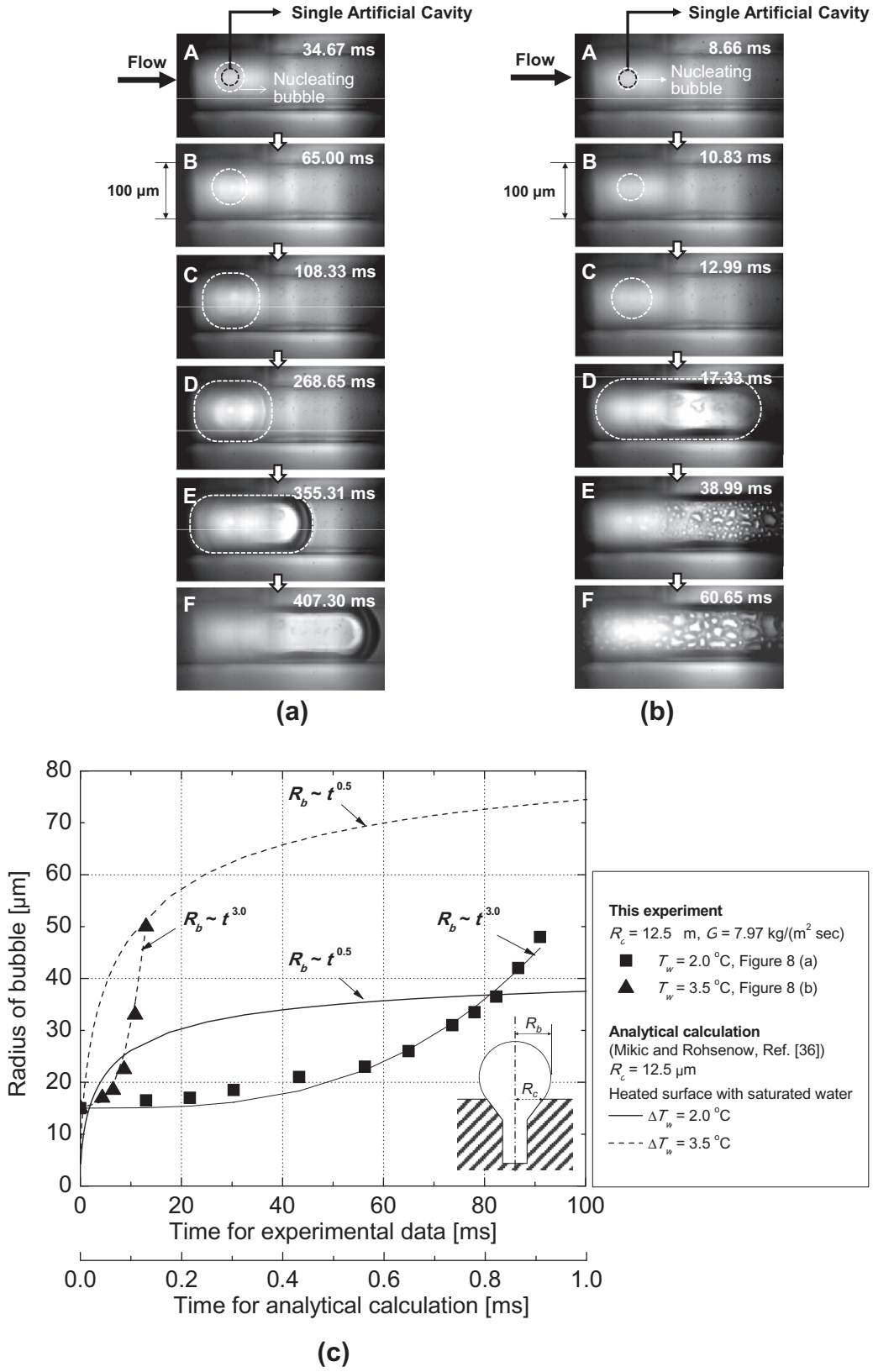

Fig. 6. Heat transfer controlled bubble growth from single artificial cavity (W = 100 μm, H = 100 μm, R_c = 12.5 μm, G = 7.97 kg/(m^2 sec)) at (a) ΔT_w = 2.0 °C and (b) ΔT_w = 3.5 °C. (c) Bubble growth rate and comparison with analytic result [36].

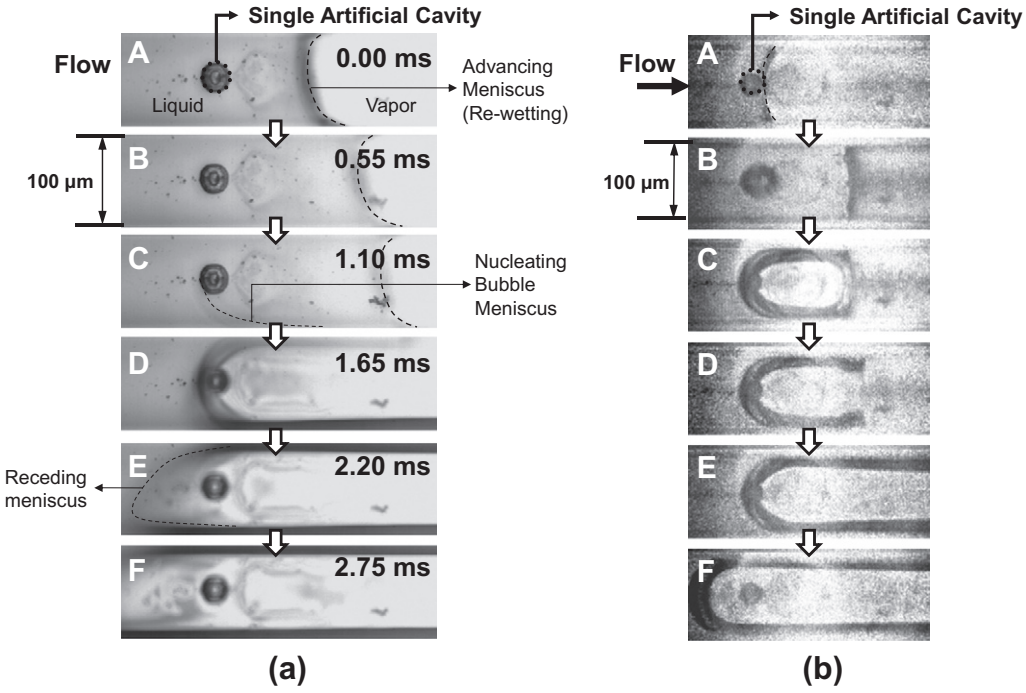

Fig. 7. Visualized sequential images of microsecond-order explosive boiling behavior from single artificial cavity (W = 100 μm, H = 48 μm, R_c = 16.4 μm, G = 31.9 kg/(m^2 s), ΔT_w = 5.6 °C): (a) commonly viewed high speed image of explosive nucleating behavior and (b) selected images of explosive nucleating images using frame straddling technique.

3.2. Heat transfer controlled bubble growth from single artificial cavity

Aforementioned cases in Section 3.1 showed local flow regime development, which helps to classify the variation of bubble growth pattern in microchannel. However, the nucleation sites of previous cases relied on natural defects, mainly at the corner of microchannel. When bubble grows from defects, it is difficult to specify the bubble nucleation and growth behavior with respect to cavity shape, cavity diameter, and wall superheat temperature. To overcome these limitations, a single artificial cavity at the bottom of the microchannel was fabricated as shown in Fig. 5. The artificial cavity was cylindrical in shape with a conical inlet. The location of cavity was chosen to be at the bottom of the microchannel and a Pt-RTD sensor was located at the backside surface of the cavity for measuring the local wall superheat temperature. The radius of cavity mouth is ranged from 12.5 to 16.4 μm.

Fig. 6 represents the visualizations of bubble growth from single artificial cavity and growth rates depending on wall superheat conditions. Although the top side Pt-RTD sensor covered the artificial cavity, the edge of the nucleating bubble could be distinguished. Images showed that the artificial cavity successfully worked as a nucleating spot, and it could provide the precise information about cavity dimension, bubble diameter and local wall temperature. Fig. 6(a) and (b) is the time lapse imagery of bubble nucleation from the artificial cavity of square microchannel (D_h = 100 μm, R_c = 12.5 μm). It had the same mass flux (G = 7.97 kg/(m^2 s)) and two different wall superheat temperature ΔT_w = 2.0 °C for Fig. 6(a) and ΔT_w = 3.5 °C for Fig. 6(b). Owing to lower mass flux than previous case, single bubble grew to the size of hydraulic diameter and expanded as capillary bubble without detachment. Before re-wetting, the flow regime then developed as annular flow with film evaporation on the nucleating spot. The time span of bubble growth was in order of milliseconds.

Using the cases of Fig. 6(a) and (b), bubble growth rate at different wall superheat temperatures could be analyzed as Fig. 6(c). From the nucleating conditions such as low superheat temperature and the millisecond order of duration of growth, this bubble growth could be considered as heat transfer controlled. However, the curve-fitted bubble radius with time is proportional to $t^{3.0}$, it means the bubble growth rate increase as the bubble size increases until the diameter reached up to the size of hydraulic diameter. From the conventional analytic calculations, uniform/non-uniform temperature field around the bubble growth rate is related with $t^{0.5}$ [35,36]. The experimental data from macrochannel also shows typical growth behavior [13]. This is attributed to the imposed limits on evaporation bubble growth by transient conduction heat transfer from the surrounded liquid to the bubble interface. Fig. 6(c) shows that growth rate had large differences between experimental curve fit and the analytical results of Mikic and Rohsenow [36]. The difference in the behavior of bubble growth under the microchannel environment as compared to the macrochannel can be attributed to differences in the local thermal and mass conditions around the bubble. In a conventional macrochannel, the bubble growth rate is affected by the presence of the bulk liquid around the bubble. However in a microchannel, the bubble is surrounded by the heated wall which presumably affects the thermal transport around the bubble. Similar bubble growth was also reported by Lee et al. [21] and Lee and Pan [22].

3.3. Explosive flow regime development and inertia controlled bubble growth

Increasing the wall superheat results in transition of bubble nucleation to a regime where bubble growth can be viewed as explosive in nature [19,22]. This behavior can be commonly seen from Fig. 7(a), where the bubble nucleation and subsequent expansion occurs in time lasting to the order of microsecond. For analyzing this behavior, single microchannel with artificial cavity (W = 100 μm, H = 48 μm and R_c = 16.4 μm) was used under the condition of G = 31.9 kg/(m^2 s) and ΔT_w = 5.6 °C. Temperature was measured at the bottom of the cavity. Imagery of Fig. 7(a) are recorded using high-speed camera with continuous light illumina-

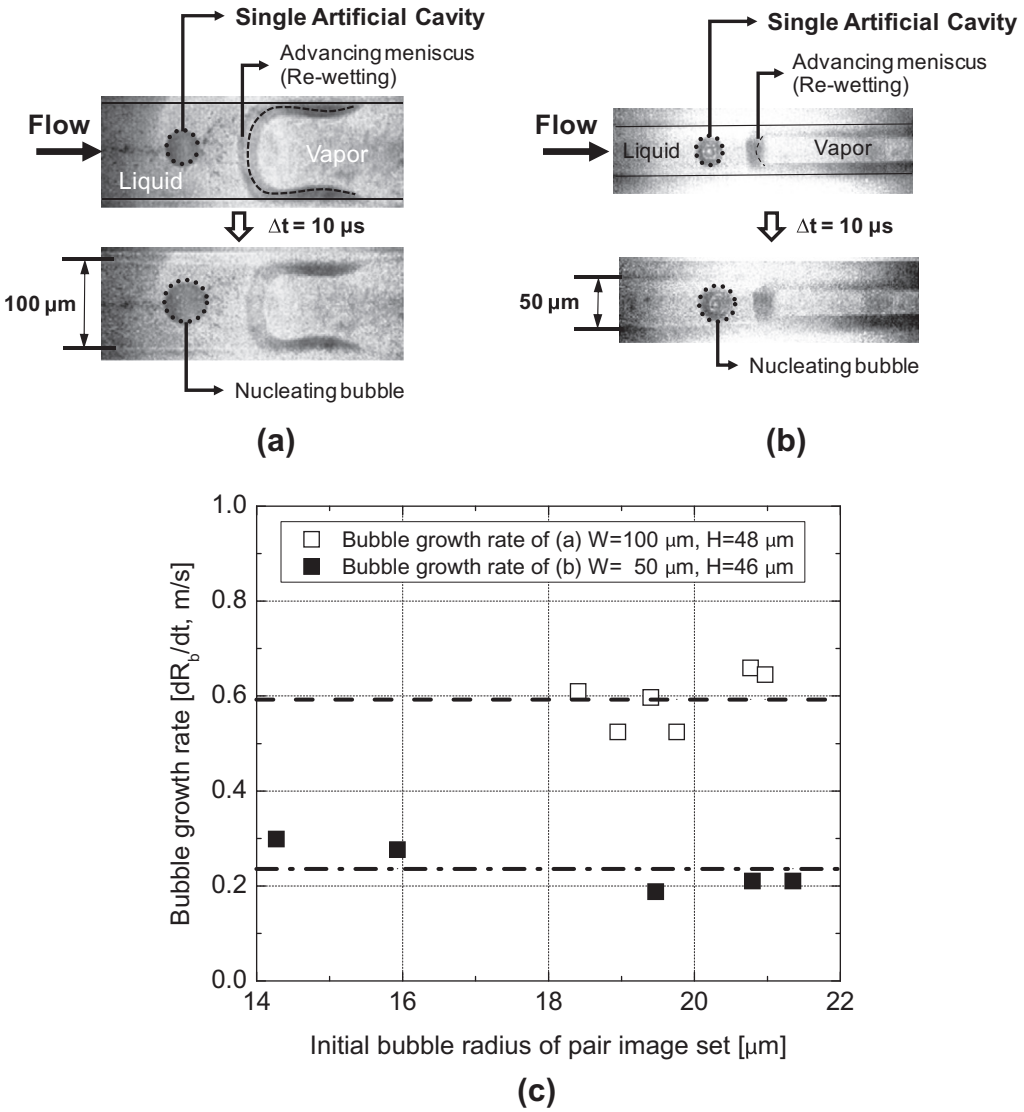

Fig. 8. Pair image set of bubble growth during 10 μs time interval and 4 ns exposure time: (a) $W = 100$ μm, $H = 48$ μm, $R_c = 16.4$ μm, $G = 31.9$ kg/(m^2 s), $\Delta T_w = 5.6$ °C, (b) $W = 50$ μm, $H = 46$ μm, $R_c = 15.3$ μm, $G = 138.9$ kg/(m^2 s), $\Delta T_w = 4.5$ °C and (c) bubble growth rate of explosive flow boiling.

tion. As can be seen from sequential images 'A–B' of Fig. 7(a), the entire process of bubble growth and expansion downstream was finished in period of 550 μs. It was clear that the process was too rapid to be investigated with 1825 FPS (frames per second) visualization. In order to acquire microsecond-order explosive bubble growth information, the visualization setup was modified. A ultra high-speed camera with frame straddling technique was synchronized with Nd:YAG laser to take two images at microsecond order time interval. Fig. 7(b) shows the selected images of explosive flow regime development at the same condition and location. It explains that single bubble is rapidly growing from the cavity shortly after re-wetting, then expands toward downstream. Bubble expansion is fast enough to meet the advancing meniscus, and flow regime is turned to annular flow then vapor expanded toward upstream. Every image was taken as a pair with a constant time interval (10 μs) and exposure time (4 ns), and they were arranged by bubble size and flow regime development. These sequential images present significant detail the bubble growth, which were then subsequently analyzed to measure their diameter as a function of time. To get the bubble growth rate on explosive boiling, two different size of microchannel were tested. One was the same as above, the other was rectangular microchannel with $W = 50$ μm and $H = 46$ μm. It had artificial cavity of $R_c = 15.3$ μm, test was conducted on the condition of $G = 138.9$ kg/(m^2 s), $\Delta T_w = 4.5$ °C. Fig. 8(a) and (b) shows one of the pair images, which were taken at a time interval of 10 μs respectively. From each set of the images, bubble growth rate could be measured. In the cases of highly explosive bubble growth, Fig. 8(c) presents that a single bubble grew linearly with time until it reached up to channel hydraulic diameter. This implies that this growth mechanism is governed by inertia controlled mechanism instead of heat transfer controlled mechanism. It means bubble growth is limited by the momentum interaction between the bubble and the surrounding liquid independent of vapor generation at the early stage of nucleation [34]. The asymptotic fit of bubble growth rate was measured as 0.59 m/s and 0.24 m/s in each case, so it took less than 100 μs to fill the entire cross-section of the channel after a bubble is nucleated from a cavity. When it was compared with analytical, inertia-limited bubble growth rate of the pool boiling (Eq. (1)) at the same thermodynamic condition, actual growth rate was smaller than calculated as 3.01 m/s and 2.76 m/s respectively [37]. Lee et al. [21] also measured bubble growth rate, however, their results

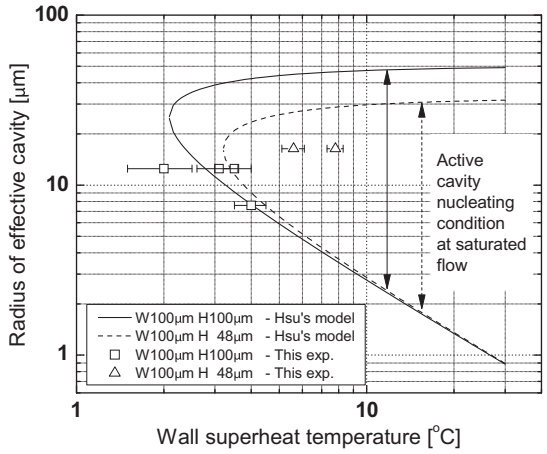

Fig. 9. Comparison between theoretical approximation of bubble nucleation with Hsu's nucleation criteria [38] for an effective range of nucleation cavity and experimental results.

were much slower than this experiment and theoretical calculations

$$\frac{dR_b}{dt} = \left[\frac{\pi}{7}\frac{(T_g - T_{sat})\rho_g i_{fg}}{T_{sat}\rho_f}\right]^{0.5} \tag{1}$$

Inertia-limited bubble growth rate can be explained by how vapor rapidly pushes the surrounding working fluid. Considering the geometrical confinement around the cavity, significant difference between measured growth rate and theoretical prediction can be related.

3.4. Incipience conditions comparison between microchannel and macrochannel

Fig. 9 shows the comparison between Hsu's macroscale theoretical nucleation criterion [35] with Kandlikar's parameter [39] and our experimental results in terms of active nucleating cavity radius and wall superheat temperature. Under the assumption that the thermal boundary layer thickness (δ_{th}) is same as the height of the microchannel, comparison between the active size range of the artificial cavity and Eq. (2) almost matches the theoretical effective cavity radius

$$\{R_{c,min}, R_{c,max}\} = \frac{\delta_{th}\sin\theta}{2.2} \times \frac{\Delta T_w}{\Delta T_w + \Delta T_{sub}}\left[1 \pm \sqrt{1 - 8.8\sigma T_{sat}\left(\frac{\Delta T_w + \Delta T_{sub}}{\rho_v h_{fg}\delta_{th}(\Delta T_w)^2}\right)}\right] \tag{2}$$

Thus, the considerable agreement between experimental results and the theory supports the idea that nucleation incipient conditions can be estimated by conventional theory to a large extent.

4. Conclusion

Microchannel flow boiling experiment under low mass flux was carried out investigating the local phenomena of flow regime development and nucleating bubble growth rate. During horizontal flow conditions, onset of nucleation, bubble growth and detachment were observed and analyzed by microscopic high-speed visualization under various flow rates and wall superheat conditions. To investigate the bubble incipient conditions and growth rate, a single artificial cavity at the bottom of the microchannel was used for generating isolated bubble and studying its subsequent growth. By associating high speed images with experimental conditions, changes of local flow boiling regime development and bubble growth rate could be observed. From the study, the following conclusions can be drawn:

- Depending on wall superheat temperature, flow regime development distinctively shows two different behaviors. The first behavior comprises of the earliest nucleating bubble detaching from the surface and thereafter sweeping downstream the channel where it coalesces with subsequent bubbles being formed in time span which is in order of milliseconds. During the second behavior, a single bubble explosively grows and expands at the nucleating spot in time span in order of microseconds. Both of these behavior show that the earliest nucleating bubble has a very important role in changing the flow regime in both cases.
- When the time span of bubble growth was in order of milliseconds, bubble growth is in the heat transfer controlled region, however, growth rate increases as the bubble radius increases. A growing bubble is presumably affected by thermal transport from the surrounding heated wall.
- The explosive bubble growth occurs within a time span of microseconds, and during this period the bubble growth rate is linear before growing to the size of the microchannel. This shows that explosive bubble nucleation is governed by inertia-controlled growth, however, growth rate is less than predicted by the conventional analytical solution.
- Nucleation incipient conditions, such as cavity radius and wall superheat temperature, are well matched with theoretical nucleation criteria. However, flow regime development and bubble growth rate does not follow similar phenomenon in macroscale flow boiling, rather it is affected by geometric constraints to a large extent.

Acknowledgement

This research was supported by the Global Partnership Program which is conducted by the Ministry of Science and Technology of the Korean Government.

References

[1] M. Iyengar, R. Schmidt, Analytical modeling for prediction of hot spot chip junction temperature for electronics cooling applications, in: ITHERM '06, 2006, pp. 87–95.
[2] K. Vasoya, Reducing hot spots and junction temperature of integrated circuits using carbon composite in a printed circuit board and substrate, in: 22nd IEEE SEMI-THERM Symposium, 2006, pp. 237–239.
[3] J.H. Kralick, US Patent No. 6355368, 2002.
[4] J.H. Lee, G.W. Skala, US Patent No. 6866955, 2005.
[5] O. Baker, Simultaneous flow of oil and gas, J. Oil Gas 53 (1954) 185.
[6] J.G. Collier, J.R. Thome, Convective Boiling and Condensation, McGraw-Hill, New York, 1981.
[7] G.F. Hewitt, Flow Regimes, Pressure Drop, Void Fraction, Handbook of Muliphase Systems, McGraw-Hill, New York, 1982.
[8] K. Cornwell, P.A. Kew, Boiling in small parallel channels, in: Proceedings of CEC Conference on Energy Efficiency in Process Technology, 1992, pp. 624–638.
[9] K.E. Kasza, M.W. Wambsganss, Flow visualization of microscale thermal mechanisms of boiling in small channels, in: Flow Visualization VII-Proceedings of the 7th International Symposium on Flow Visualization, 1995, pp. 262–267.
[10] K.E. Kasza, M.W. Wambsganss, Microscale flow visualization of nucleating boiling in small channels mechanisms influencing heat transfer, in: Proceedings of International Conference on Compact Heat Exchangers for the Process Industries, 1997, pp. 343–352.
[11] S.G. Kandlikar, M.D. Cartwright, V.R. Mizo, A photographic study of nucleation characteristics of cavities in flow boiling, in: Proceedings of Convection Flow Boiling, An International Conference, Banff, Canada, 1995, pp. 73–78.
[12] S.G. Kandlikar, V.R. Mizo, M.D. Cartwright, Investigation of bubble departure mechanism in subcooled flow boiling of water using high speed photography,

in: Proceedings of Convection Flow Boiling, An International Conference, Banff, 1995, pp. 161–166.
[13] S.G. Kandlikar, V.R. Mizo, M.D. Cartwright, E. Ikenze, Bubble nucleation and growth characteristics in subcooled flow boiling of water, in: HTD-Vol. 342, National Heat Transfer Conferences, vol. 4, 1997, pp. 11–18.
[14] P. Balasubramanian, S.G. Kandlikar, High speed photographic observation of flow patterns during flow boiling in single rectangular minichannel, in: ASME Summer Heat Transfer Conference, Las Vegas, HT2003-47175, 2003, pp. 1–7.
[15] M.E. Steinke, S.G. Kandlikar, Flow boiling and pressure drop in parallel flow microchannels, in: 1st International Conference on Microchannels and Minichannels, Rochester, ICMM2003-1070, 2003, pp. 1–13.
[16] L. Jiang, M. Wong, Y. Zohar, Phase change in microchannel heat sink under forced convection boiling, in: Proceedings of 13th Annular International Conference on Micro Electro Mechanical Systems, Miyazaki, Japan, 2000.
[17] L. Jiang, M. Wong, Y. Zohar, Forced convection boiling in a microchannel heat sink, J. Microelectromech. Syst. 10 (1) (2001) 80–87.
[18] L. Zhang, E.N. Wang, K.E. Goodson, T.W. Kenny, Phase change phenomena in silicon microchannel, Int. J. Heat Mass Transfer 48 (8) (2005) 1572–1582.
[19] G. Hetsroni, A. Mosyak, E. Pogrebnyak, Z. Segal, Explosive boiling of water in parallel micro-channels, Int. J. Multiph. Flow 31 (2005) 371–392.
[20] D. Liu, P.S. Lee, S.V. Garimella, Prediction of the onset of nucleate boiling in microchannel flow, Int. J. Heat Mass Transfer 48 (2005) 5134–5149.
[21] P.C. Lee, F.G. Tseng, C. Pan, Bubble dynamics in microchannels. Part I: Single microchannel, Int. J. Heat Mass Transfer 47 (2004) 5575–5589.
[22] P.C. Lee, C. Pan, On the eruptive boiling in silicon-based microchannels, Int. J. Heat Mass Transfer 51 (2008) 4841–4849.
[23] G. Liu, J. Xu, Y. Yang, Seed bubbles trigger boiling heat transfer in silicon microchannels, Microfluid. Nanofluid. 8 (2010) 341–359.
[24] S.G. Kandlikar, W.K. Kuan, D.A. Willistein, J. Borrelli, Stabilization of flow boiling in microchannels using pressure drop elements and fabricated nucleation sites, J. Heat Transfer 128 (2006) 389–396.
[25] C.J. Kuo, Y. Peles, Local measurement of flow boiling in structured surface microchannel, Int. J. Heat Mass Transfer 50 (2007) 4513–4526.
[26] C.T. Lu, C. Pan, A highly stable microchannel heat sink for convective boiling, J. Micromech. Microeng. 19 (2009) 055013.
[27] J.Y. Lee, K.I. Cho, I.S. Song, C.B. Kim, S.Y. Son, Microscale bubble nucleation from an artificial cavity in single microchannel, J. Heat Transfer 125 (2003) 545.
[28] F.D. Moore, R.B. Mesler, Measurement of rapid surface temperature fluctuations during nucleate boiling of water, AIChE J. 7 (4) (1961) 620–624.
[29] C. Bongiovanni, A. Dominguez, J-P. Chevaillier, Understanding images of bubbles, Eur. J. Phys. 21 (6) (2000) 561–570.
[30] V.P. Carey, Liquid-Vapor Phase-Change Phenomena, Taylor & Francis, Bristol, PA, 1992. pp. 404–411.
[31] C.T. Crowe, Multiphase Flow Handbook, CRC Press, 2005. pp. 3–7.
[32] S.G. Kandlikar, A mechanistic model for saturated flow boiling heat transfer, in: ASME Winter Annual Meeting, ASME-HTD.145, 1990, pp. 61–69.
[33] X. Fu, C.J. Huang, R.Z. Wang, Bubble growth, departure and the following flow pattern evolution during flow boiling in mini-tube, Int. J. Heat Mass Transfer 53 (2010) 4819–4831.
[34] J.R. Thome, V. Dupont, A.M. Jacobi, Heat transfer model for evaporation in microchannels. Part I: Presentation of the model, Int. J. Heat Mass Transfer 47 (2004) 3375–3385.
[35] M.S. Plesset, S.A. Zwick, The growth of vapor bubbles in superheated liquids, J. Appl. Phys. 25 (1954) 493–500.
[36] B.B. Mikic, W.M. Rohsenow, Bubble growth rates in non-uniform temperature field, Prog. Heat Mass Transfer 2 (1969) 283–292.
[37] B.B. Mikic, W.M. Rohsenow, P. Griffith, On bubble growth rates, Int. J. Heat Mass Transfer 13 (4) (1970) 657–666.
[38] Y.Y. Hsu, On the size range of active nucleation cavities on a heating surface, J. Heat Transfer 41 (1962) 207–216.
[39] S.G. Kandlikar, Nucleation characteristics and stability considerations during flow boiling in microchannels, Exp. Therm. Fluid Sci. 30 (2006) 441–447.